Resolving Challenges of Mass Transport in Non Pt-Group Metal Catalysts for Oxygen Reduction in Proton Exchange Membrane Fuel Cells

Ryan Pavlicek,[1,*] Scott Calabrese Barton,[2,*] Nathaniel Leonard,[2,a] Henry Romero,[3] Sam McKinney,[3] Geoffrey McCool,[3] Alexey Serov,[3,4,*] Daniel Abbott,[1,*,b] Plamen Atanassov,[4,] and Sanjeev Mukerjee[1,**,z]**

[1]*Northeastern University Center for Renewable Energy Technology (NUCRET), Department of Chemistry and Chemical Biology, Northeastern University, Boston, Massachusetts 02115, USA*
[2]*Chemical Engineering and Materials Science, Michigan State University, East Lansing, Michigan, 48824, USA*
[3]*Pajarito Powder, Albuquerque, New Mexico 87109, USA*
[4]*Department of Chemical and Biological Engineering, University of New Mexico, Albuquerque, New Mexico 87131, USA*

Mass transport properties of a pair of non-Platinum Group Metal (non-PGM) catalysts in proton exchange membrane fuel cells (PEMFCs) were evaluated through methods developed by Reshetenko et al., demonstrating that the use of different carrier gases can allow for the determination of the mass transport coefficient for oxygen in the gas phase and the electrolyte phase. The gas-phase and non-gas-phase resistances can be elucidated from the slope and intercept, respectively, of the total mass transport coefficient plotted as a function of molecular weight. It was determined through these experiments that the primary sources of mass transfer limitations of the non-PGMs when compared to the PGMs were the catalyst layer (non-gas-phase), rather than the flow fields (gas-phase, primarily Knudsen Diffusion effects), and the gas diffusion layer. This work was combined with a pseudo-2D, isothermal, steady state numerical model to estimate the gas-phase mass transfer coefficient and the fraction of hydrophobic, gas-phase pores in the catalyst layer. Sensitivity studies were also carried out, allowing for more information regarding the influence of several inherent factors on the mass transport limitations, and allow for additional validation of the model beyond simply the quality of the fit.
 [DOI: 10.1149/2.0141809jes]

Manuscript submitted September 5, 2017; revised manuscript received May 11, 2018. Published May 26, 2018. This was Paper 1297 presented at the Phoenix, Arizona, Meeting of the Society, October 11–15, 2015.

Today's growing demand for alternative and clean power generation has led to increased research into proton exchange membrane fuel cells (PEMFCs) due to their high efficiency and theoretical power density. While the current state-of-the-art catalyst for both the Hydrogen Oxidation Reaction (HOR) and Oxygen Reduction Reaction (ORR) in such cells is platinum, the cost of said catalyst remains one of the largest obstacles preventing mass commercialization, with a resolution requiring either a reduction in platinum loading[1–4] or a less costly catalyst. In recent years, major breakthroughs have been achieved in the development of non-platinum group metal (non-PGM) catalysts for ORR.[5–20] These catalysts primarily relied upon the presence of nitrogen-coordinated active sites, and oftentimes the presence of a transition metal such as iron or cobalt. The catalysts in this work were derived from one of two distinct synthetic approaches. The first requires the pyrolysis of a ferrous iron salt and a nitrogen-containing charge-transfer salt followed by the etching of a silica template to form a metal-nitrogen-carbon structure.[21–23] The second strategy utilizes the formation of a metal-organic-framework (MOF), which, upon pyrolysis, forms a highly active catalyst towards ORR that remains devoid of any direct coordination of iron to nitrogen.[24] Both of these materials were shown to have very high ORR activity in acid media and subsequently in PEMFCs.

While much has been elucidated regarding the mechanism of ORR in both acidic and alkaline media with regards to both PGM and non-PGM,[25] mass transfer factors remain an important but less studied area of fuel cell technology. Baker et al. studied mass transport as a function of oxygen partial pressure and identified pressure-dependent and –independent components of the mass transfer coefficient.[26–28] This approach has been applied to estimate a Nafion barrier thickness for low-loading Pt cathodes.[29] Recently, however, Reshetenko et al. reported experiments in which a wide range of inert gases were used as diluents in the cathode feed.[30–32] The variation of the carrier gases will alter the diffusivity of oxygen, which will subsequently facilitate experimental calculation of the gas-phase transport resistance. The only instances of these studies to date revolved around platinum electrodes, while this work will aim to expand beyond that to various non-PGM catalysts.

The goal of the study by Reshetenko et al.[30] was to vary the gas-phase mass transfer coefficient of oxygen in the cathode by varying the molecular weight of the carrier gas. For a cathode exhibiting first order kinetics with respect to oxygen, the average cathode limiting current, i_{ave}, was shown to vary as:

$$\ln\left(1-\frac{i_{ave}}{i_e}\right) = -\frac{nFkp_r}{RT}\cdot\frac{1}{i_e f} \quad [1]$$

where i_{ave} is the average limiting current, i_e is the stoichiometric limiting current determined by the gas flow rate, n is the electron transfer coefficient (4 for O_2 reduction to water), F is Faraday's constant, k is the mass transfer coefficient for delivery of oxygen to the electrode, p_r is the dry inlet reactant partial pressure, R is the gas constant, and T the temperature. By measuring i_{ave} experimentally and calculating i_e, one can plot the left side of Eq. 1 as a function of $(i_e f)^{-1}$, which should yield a linear relationship with negative slope, passing through the origin. Knowing the other parameters, this slope can be used to estimate the mass transfer coefficient, k. It is expected that this coefficient is dependent on the diffusivity of O_2 in the carrier gas, but also depends on other mass transfer limitations such as Knudsen diffusion, transport through the ionomer, the presence of vapor-phase and liquid water, etc.

Previously, a one-dimensional, isothermal model was designed for steady-state characterization of non-PGM PEMFCs.[33] This model included consideration of multiphase transport in the catalyst layer of a relatively thick non-PGM oxygen diffusion cathode. Gas-phase transport included consideration of Knudsen diffusion, and the model was able to account for hydrophilicity and pore-size distribution, which could be correlated to flooding within the catalyst layer. Due to the

*Electrochemical Society Member.
**Electrochemical Society Fellow.
[a]Present Address: The Electrochemical Energy, Catalysis, and Materials Science Laboratory, Department of Chemistry, Chemical Engineering Division, Technical University Berlin, 10623 Berlin, Germany.
[b]Present Address: Electrochemistry Laboratory, Paul Scherrer Institut, CH-5232 Villigen PSI, Switzerland.
[z]E-mail: s.mukerjee@neu.edu

use of a low concentration oxygen cathode gas in the present study, it cannot be assumed that the oxygen concentration remains constant over the length of the serpentine flow fields. The model was therefore adapted into a pseudo two-dimensional system, in which the oxygen concentration varies along the flow field path. Sensitivity studies, described in more detail later, were also carried out. These studies allowed for a more concrete evaluation of the effect of modifications within the system upon the mass transport limitations.

This work demonstrates the first use of these mass transport experiments on various high-performing non-PGM catalysts. The combination of these experimental results with the adaptation of the previously-mentioned model into a pseudo two-dimensional system is used to yield previously unattainable information on the catalyst layer and its transport characteristics.

Experimental

Catalyst/MEA preparation and testing.—Catalyst synthesis using the silica-etching method (referred to hereon as NPC-2000) was performed by Pajarito Powder (Albuquerque, NM), using a proprietary scale-up method based on the originally published method at University of New Mexico.[22] GDEs were constructed onsite at Pajarito Powder and subsequently provided to Northeastern University for Membrane Electrode Assembly (MEA) preparation and testing.

The MOF catalyst in question (hereon referred to as MOF SR) was synthesized through a previously-published technique.[24] In one flask, 2-methylimidazole is dissolved in room temperature methanol, while in another, 1,10-phenanthroline monohydrate and zinc(II) nitrate *x*-hydrate are dissolved in room temperature water. When both dissolutions are complete, the aqueous solution is poured into the methanol solution, followed by the addition of iron(II) acetate, and stirred for an additional 24 hours. Following a series of centrifuging steps and methanol washes, the resulting solid are dried in a vacuum oven, prior to being subjected to a pair of heat treatments. The first takes place in an argon environment at 1050°C (1hr dwell time), followed by a second pyrolysis in an ammonia environment, also at 1050°C (18min dwell time).

Cathode electrodes were prepared at NEU using the commercially available Sigracet 25BC gas diffusion media (Ion Power). Catalyst inks were made by mixing 55mg non-PGM catalyst, 900mg of a 5% Nafion (Dupont, USA) dispersion (Alfa Aesar), 8.5mL IPA, and 1.5mL H_2O. The ink was homogenized (IKA T25) for 1hr at 17000rpm while held in an ice bath. Catalyst layers were applied by use of a spray gun (IWATA HP-BCS) to the aforementioned GDL. Commercially available GDEs with loadings of 0.4mg$_{Pt}$/cm^2 (Johnson Matthey ELE0162) were used as anodes. Catalyst loading of the non-PGM electrodes was 2mg/cm^2. Nafion contact layers of 0.5mg/cm^2 were applied to both electrodes. Electrodes were hot-pressed with Nafion 211 membrane at 130°C for 5 minutes under 400psi pressure. Electrodes measured 4.62cm^2 in active area (2.1cm × 2.2cm). For the platinum reference cell, the same commercially available GDE was used as the anode. A similar procedure as for the non-PGM was used to spray the platinum cathode, using commercial 46.2% Pt/C (Tanaka Kikinzoku International KK, Japan). Final cathode loading of the Pt reference cell was 0.36mg$_{Pt}$/cm^2.

Electrodes prepared from the above inks were characterized for pore size distribution using mercury intrusion porosimetry (MIP, Micromeritics AutoPore IV 9500). Samples were prepared by spraying the catalyst ink onto a heated glass plate. Upon drying the material was removed using a blade. A penetrometer of 3mL total volume and 1.1mL stem volume was loaded with 0.1g of catalyst layer (CL) material. Mercury intrusion volume was obtained for pressures of 0.1 to 30000psia. The pore radius, r_p, was obtained from the pressure, p, via the Washburn equation[34]

$$r_p = \frac{2\gamma cos\theta}{p} \quad [2]$$

with a contact angle $\theta = 130^\circ$ and mercury surface tension $\gamma = 485$dyn/cm.

Standard 5cm^2 cell housings from Fuel Cell Technologies were used with serpentine flow fields. Mass transport experiments were conducted with the cell temperature held at 80°C and 100% relative humidity (achieved through heating the water tanks to 85°C), with 7psi of backpressure applied. Flow rates were designed with a ratio shown to facilitate water transport.[30] Cathode gases were all 4% oxygen, diluted with argon, nitrogen, or helium. Polarization curves and Electrochemical Impedance Spectroscopy (EIS) spectra were taken potentiostatically using a Metrohn Autolab (PGSTAT302N) in conjunction with a 20A current booster (PGSTAT30) and associated NOVA software.

Model development.—The numerical model applied in this work is based on the one-dimensional model of the catalyst layer/gas diffusion layer previously published.[33] The model was adapted to a pseudo-two-dimensional system by inclusion of compositional changes along the flow channel. In essence, the model becomes a one dimensional, isothermal, steady-state model where the independent variable is position along the flow channel and a source term represents depletion of oxygen in the channel. Additionally, a catalyst particle-scale mass transfer term, k_{MT}, was added to consider local mass transfer effects.

Variation of oxygen molar flow rate, F_O, with position along the flow channel, z, was determined using a first order mole balance:

$$\frac{dF_O}{dz} = j_O W \;\; ; \;\; F_O|_{z=0} = \frac{x_O P v}{RT} \quad [3]$$

where j_O is the local flux of oxygen into the flow field due to reaction within the electrode. This local flux is calculated using the one-dimensional electrode/GDL model.[33] The effective channel width, W, includes channel and lands, and is calculated from the flow field area, A, and channel length, L, by $W = A/L$. The initial value of F_O is given by the pressure, P, the volume flow rate, v, the mole fraction of oxygen, x_O, and the temperature, T, where R is the gas constant.

The channel flow also comprised water vapor, diluent gas (helium, argon, or nitrogen), and liquid water. Because the diluent was not involved in electrode reactions, the diluent flux, F_d, was considered constant, or $dF_d/dz = 0$. This assumption also considers crossover flux of diluent to the anode to be negligible. The flow was considered to be saturated throughout the channel, such that for constant temperature and pressure, the vapor-phase mole fraction of water, x_w, was considered constant. In the model, this was enforced with the equation:

$$\frac{dF_w}{dz} = \frac{x_w}{1 - x_w}\left(\frac{dF_O}{dz} + \frac{dF_d}{dz}\right) \quad [4]$$

At any point in the flow field, the mole fraction, x_i, of any component i can be calculated from $x_i = F_i/F_T$, where F_T is the total molar flow rate $F_T = \sum F_i$. For simplicity, liquid water content in the flow channel was ignored, because of its low molar volume (0.019 L/mol compared to 29 L/mol for water vapor).

Local mass transfer was considered by introduction of a mass transfer coefficient, k_{MT}, in parallel with the ORR reaction. In this way, the local volume-specific reaction rate, r_{ORR} (mol cm^{-3} s^{-1}) can be written as

$$r_{ORR} = \frac{k_{ORR} x_O}{1 + k_{ORR}/k_{MT}} \quad [5]$$

where k_{ORR} (mol cm^{-3} s^{-1}) is volumetric rate constant that is a function of local conditions such as potential, and x_O is the local oxygen mole fraction.[33] In addition to k_{MT}, the catalyst layer exchange current density (i_0, A cm^{-3}), catalyst layer ionic conductivity (κ, mS cm^{-1}), and catalyst layer hydrophobic fraction (f_{HO}) were used as adjustable parameters to fit experimental data.[33] The catalyst layer hydrophobic fraction refers to the hydrophobic pore fraction. Hydrophobic pores have water contact angle greater than 90° and are filled with a combination of water and gas, depending on the level of saturation. These can be distinguished from hydrophilic pores of low contact angle that are water-filled.[33]

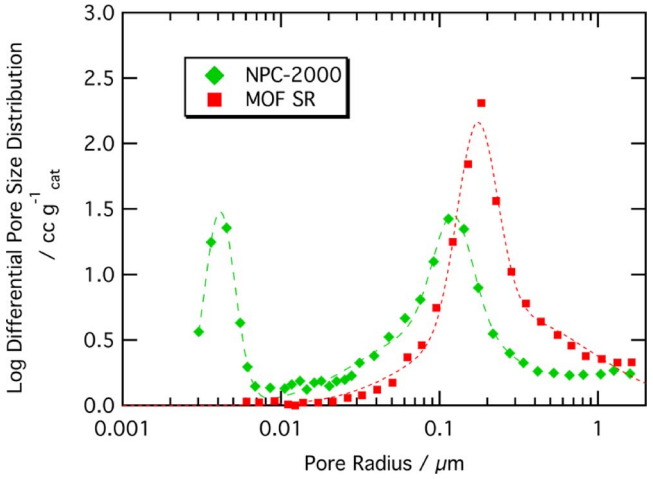

Figure 1. Pore size distributions by mercury intrusion porosimetry (MIP) for catalyst layers prepared from NPC-2000 and MOF SR catalyst materials, reproduced with permission.[39] Dashed lines indicate deconvolution of distributions into three (NPC-2000)[33] and two (MOF SR) log-normal distributions with mean radius, r_0, and volume fractions indicated in the table.

The model was parameterized as follows: The flow field was treated as a rectangular channel of length $L = 18$ cm and corresponding to the cell area $A = 5$ cm^2. Pore size distributions were taken from mercury porosimetry data (Fig. 1) for each catalyst. Diffusivities of oxygen and water in the three carrier gases (He, Ar, N_2) were calculated from correlations at 80°C, yielding the values shown in Table II.[35,36] With the exception of the adjustable parameters noted above, all other parameters are taken from the original one-dimensional model.[33]

For a first order process of rate kC (mol L^{-1} s^{-1}) in an ideal plug flow reactor, the integral form of the material balance can be expressed as[37,38]

$$\tau = C_0 \int_0^X \frac{dX}{kC} \qquad [6]$$

where $\tau = V/v$ is the reactor space time with V reactor volume and v volume flow rate, C is the reactant concentration with inlet value C_0, k is a first-order rate constant and X is the fractional conversion of reactant, equivalent to i_{avg}/i_e. For a gas phase reactor, C can be written as $C_0(1 - \epsilon X)$ and Eq. 6 integrated to yield

$$\tau k = \frac{1}{k}\left[(1+\epsilon)\ln\left(\frac{1}{1-X}\right) - \epsilon X\right] \qquad [7]$$

The parameter ϵ is related to gas expansion due to reaction, and can be expressed as $y_0\delta$, where y_0 is the initial mole fraction of reactant and δ is the molar change of reaction.[37] For cathodic oxygen reduction to water, $\delta = 1$. In these experiments, $y_0 \ll 1$, and so $\epsilon \sim 0$ and Eq. 7 reduces to

$$\ln(1 - x) = -\tau k \qquad [8]$$

Eq. 8 is equivalent to Eq. 1. If the first-order process consists of a mass transfer and reaction step in series, the rate constant k expands to associated constants k'_g and k_0 according to

$$\frac{1}{k} = \frac{M}{k'_g} + \frac{1}{k_0} \qquad [9]$$

Here we have assumed that the mass transfer constant depends linearly on carrier gas molecular weight, M, as proposed by Reshetenko et al. Based on this analysis, we can ascribe the slope k'_g to gas-phase dependent phenomena, and k_0 to gas-phase independent phenomena. The latter can include reaction kinetics, Knudsen diffusion, and diffusion through water in either liquid or vapor phases.

Model fitting to experimental data.—The pseudo 2-D numerical model was used to analyze the experimental data by fitting. Differing pore size distributions were used to distinguish between the NPC-2000 and MOF SR catalysts, and a subset of polarization data (100 uniformly distributed points out of the ~400 points collected) were chosen under both helium and argon and for all flow rates (Fig. 2). These data were fit by the model using the nonlinear Levenberg-Marquardt algorithm, with uniform weighting, as implemented in the MATLAB function NLINFIT, and used three fitting parameters: ionic conductivity, exchange current density, and hydrophobic porosity. Separate parameter estimates were obtained for the NPC-2000 and MOF SR catalysts.

Table I. Pore Size Results for Fig. 1.

NPC-2000		MOF SR	
r_0/nm	Volume Fraction	r_0/nm	Volume Fraction
4.1	0.27	173	0.36
98	0.52	277	0.64
121	0.21		

Model sensitivity studies.—Sensitivity was calculated by running the model at a fixed step size of 10% for a given parameter. The change in a dependent variable, Δy, due to a change, Δx, in the value of a parameter x, leads to the sensitivity, B_x:

$$B_x = \frac{\Delta y / y}{\Delta x / x} \qquad [10]$$

A positive sensitivity indicates a correlation between current and the parameter of interest, whereas a negative value indicates anti-correlation. No correlation is indicated by a sensitivity of zero.

Simulations were conducted using the MOF SR catalyst at 0 V cell potential for both argon and helium carrier gases, for cathode gas flow rates of 45–136 sccm. A linear fit to the resulting value of the mass transfer coefficient, k, was obtained as shown in Fig. 6. Sensitivity of the resulting dependent variables k_0 and k'_g were calculated according to Eq. 10.

Pore size distributions.—Pore size distributions determined by mercury intrusion porosimetry are displayed in Fig. 1, with tabulated pore modes for each catalyst shown in Table I.[39] The NPC-2000 materials demonstrated a significant pore mode length scales below 10 nm, but no such mode was observed in the MOF SR catalyst. Both catalysts exhibited significant pore volume in the 100–300 nm range. These distributions were used as inputs to the pseudo-two dimensional numerical model.

Results – HelOx Testing

Fuel cell polarization studies were conducted using membrane-electrode assemblies (MEAs) with 4% O_2 in helium, argon, and nitrogen carrier gases at 80°C and various cathode feed flow rates. Three catalyst materials that were considered were a Tanaka carbon-support Pt catalyst (46.2 wt% Pt), and non-PGM catalysts based on either a metal-organic-framework (MOF SR) or charge-transfer salt (NPC-2000) precursors. Cathode feed flow rates were chosen to maximize the range of O_2 utilization for each catalyst.

Fig. 2 shows polarization curves for the MOF SR and NPC-2000 catalysts for varying flow rates in the three carrier gases. Equivalent data for the Pt reference electrode is provided in Supporting Information. One can see that the current densities obtained for the NPC-2000 catalyst were somewhat higher and more influenced by feed flow rate. Therefore the range of flowrates chosen for the MOF SR catalyst overlaps with the NPC-2000 catalyst but are somewhat higher. At low potentials (approaching 0.1 V), the polarization curves approach mass-transfer limited plateaus where current density becomes independent of cell potential.

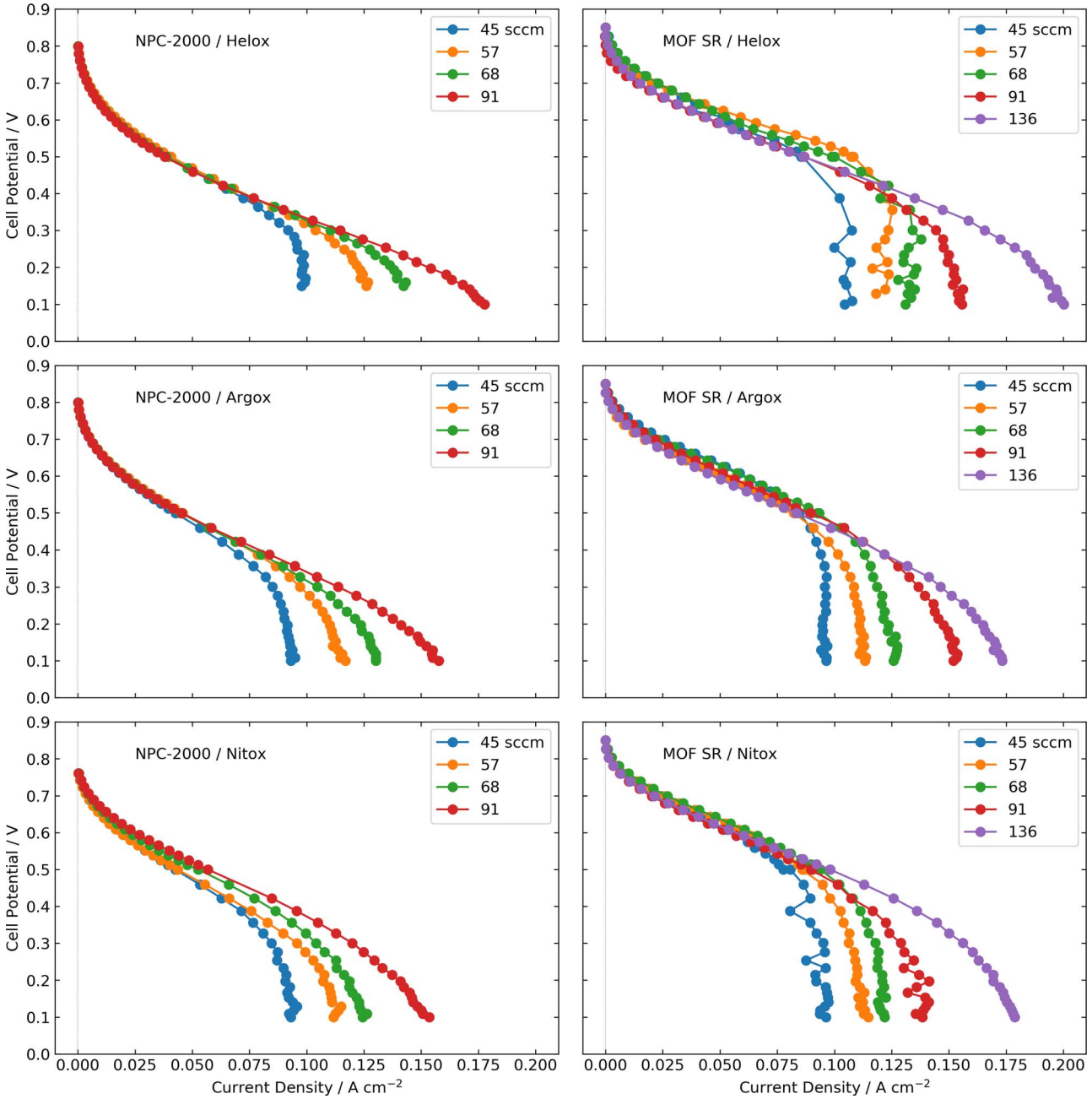

Figure 2. Polarization curves for MOF SR and NPC-2000 catalysts at various flow rates, 80°C, 100%RH, 2mg/cm^2 catalyst loading.

Mass-transfer limited current densities were estimated for each catalyst and flow rate and are shown in Fig. 3, where the limiting currents are represented according to Eq. 1. Here, for each diluent gas, the logarithmic function varies approximately linearly with the inverse of the stoichiometric current density. Lower values of the logarithmic function represent exponentially increased utilization of oxygen at the cathode. This function tends to depart from linearity toward the right of the plot, representing extremely low flow rates. This behavior is consistent with studies on PGM-based electrodes.[30] Also in Fig. 3, a linear fit is applied to each data set in order to determine the slope, $-nFkp_r/RT$, in Eq. 1. In adherence to Eq. 1, the fitting function is assumed to have zero intercept, and therefore passes through the origin of the plot. Moreover, the rightmost data point is excluded from the fit in order to emphasize the linear region.

The resulting mass transfer coefficients are tabulated in Table II. These values were calculated at 80°C and 21.7 psi absolute pressure (7 psi back pressure) with $n = 4$. It can be seen that the values of k are consistent between the two catalysts, with $k \approx 3.0$ m s^{-1} for helium and $k \approx 2.5$ m s^{-1} for argon and nitrogen. Despite the fact that the experimental data does not obviously tend toward the origin for high flow rates, the error estimates for k are reasonably low.

Overall mass transfer resistance in the CL+GDL may be considered as a series combination of gas-phase resistance, R_g, and non-gas-phase resistance, R_0:

$$R_{MT} = \frac{L}{kA} = R_g + R_0 = \frac{L}{k_g A} + \frac{L}{k_0 A} \quad [11]$$

such that the overall mass transfer resistance, k, consists of gas-phase and non-gas-phase components:

$$\frac{1}{k} = \frac{1}{k_0} + \frac{1}{k_g} \quad [12]$$

Table II. Calculated Mass Transfer Coefficients.

Diluent	MW_d g mol^{-1}	D_{O_2} cm^2 s^{-1} @ 80°C[30,36,40]	D_{H_2O} cm^2 s^{-1} @ 80°C[35]	k/m s^{-1} × 10^3 MOF SR	k/m s^{-1} × 10^3 NPC-2000
Helium	4.0	0.994	1.115	2.9 ± 0.05	3.0 ± 0.11
Argon	39.9	0.259	0.361	2.4 ± 0.11	2.5 ± 0.11
Nitrogen	28.0	0.283	0.358	2.4 ± 0.07	2.4 ± 0.09

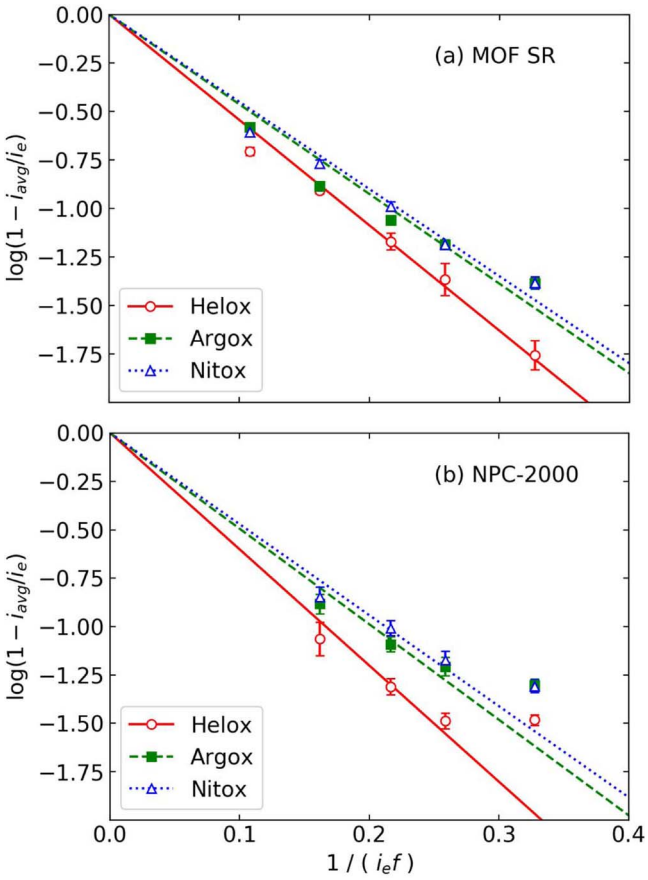

Figure 3. Limiting current plotted in log form relative to stoichiometric current density i_{ef} for MOF SR (a) and NPC-2000 (b). Plotted in this way, the slope of fitted lines provides an estimate of mass transfer coefficient, k.

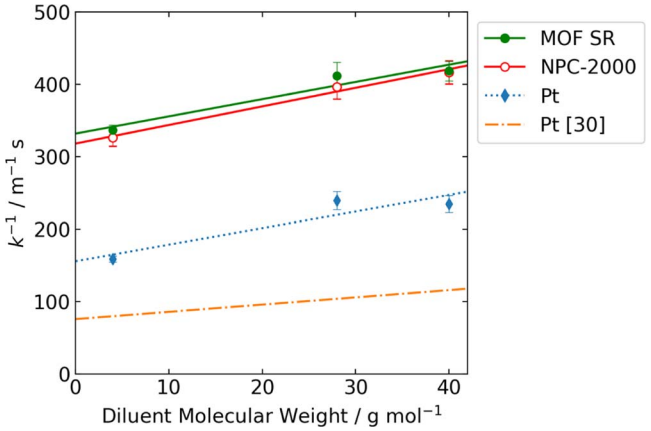

Figure 4. Dependence of mass transfer coefficient, k, on diluent molecular weight. Extrapolation of 1/k to the vertical axis yields an estimate of $1/k_0$.

where the value of k_g depends linearly on the diffusivity of oxygen in the diluent gas. Following Reshetenko et al., we infer that the second term in Eq. 12 is linearly proportional to diluent molecular weight, MW_d. We therefore plot the data in Table II as a function of MW_d in Fig. 4.

As mentioned above, the values of k for the non-PGM catalysts MOF SR and NPC-2000 are comparable, and their slope and intercept are similar, within error. These results are depicted in Table III. These slopes are also comparable to the slope obtained for the Pt-catalyzed electrode. This is indicative of the non-PGM materials demonstrating similar gas-phase mass transport resistances to the Pt cells. This is heavily dependent on the path of gas transport, which in turn is heavily influenced by the gas diffusion media. Both the PGM and non-PGM MEAs were fabricated using similar gas diffusion media. Therefore, it is unsurprising that for a non-PGM and Pt systems that utilized the same diluent gases, the gas-phase resistance would be similar. The intercept of these curves is most significant, as it represents $1/k_0$. The intercepts for the non-PGM electrodes are comparable, and are dramatically higher than those of the Pt electrode, representing significantly lower values of k_0. Beyond a potentially inherent higher mass transport resistance of the non-PGM materials, the non-PGM catalyst layers are significantly thicker (roughly two-fold), and this is believed to play a significant role in the increased resistance demonstrated in the non-PGM materials than is present in both Pt standard MEAs.

Model Results

The pseudo 2-D numerical model was used to analyze the experimental data by fitting. Differing pore size distributions were used to distinguish between the NPC-2000 and MOF SR catalysts, and a subset of polarization curves under helium and argon (Fig. 2) were fit with a nonlinear algorithm, using three fitting parameters: ionic conductivity, exchange current density, and hydrophobic porosity. These parameters were chosen to further distinguish the two catalysts on the basis of kinetics, ionic transport, and gas-phase transport. For each catalyst, parameters were obtained that best fit polarization curves under both helium and argon for four to five gas flow rates, such that 6 polarization curves were simultaneously fitted. Data under nitrogen was not fit due to its similarity to argon data. Fitting results are shown in Fig. 5, and the fitted parameter values, are given in Table IV. Again, the value of $1/k_0$ was analyzed as a function of the diluent molecular weight, and the results of those are shown in Fig. 6.

Comparing the two catalysts, the catalyst layer conductivity, κ, and exchange current density, i_0, are similar, within fairly large confidence interval (∼20%). Such large intervals (low confidence) reflects the primarily mass-transfer controlled nature of these experiments. However, the i_0 and κ values for MOF SR are 10% and ∼29% higher than that of NPC-2000, respectively, accounting for the decreased observed high-potential polarization observed for MOF SR. The fitted

Table III. Regression Results for Fig. 4.

Catalyst	Slope m^{-1} s g^{-1} mol	Intercept m^{-1} s	k_0 m s^{-1} × 10^3
MOF SR	2.16 ± 0.4	355 ± 11	2.8 ± 0.17
NPC-2000	2.57 ± 0.32	318 ± 9.0	3.1 ± 0.09
Pt	2.3 ± 0.93	156 ± 26	6.4 ± 1.1
Pt[30]	1.0 ± 0.084	78 ± 7.7	12.8 ± 1.3

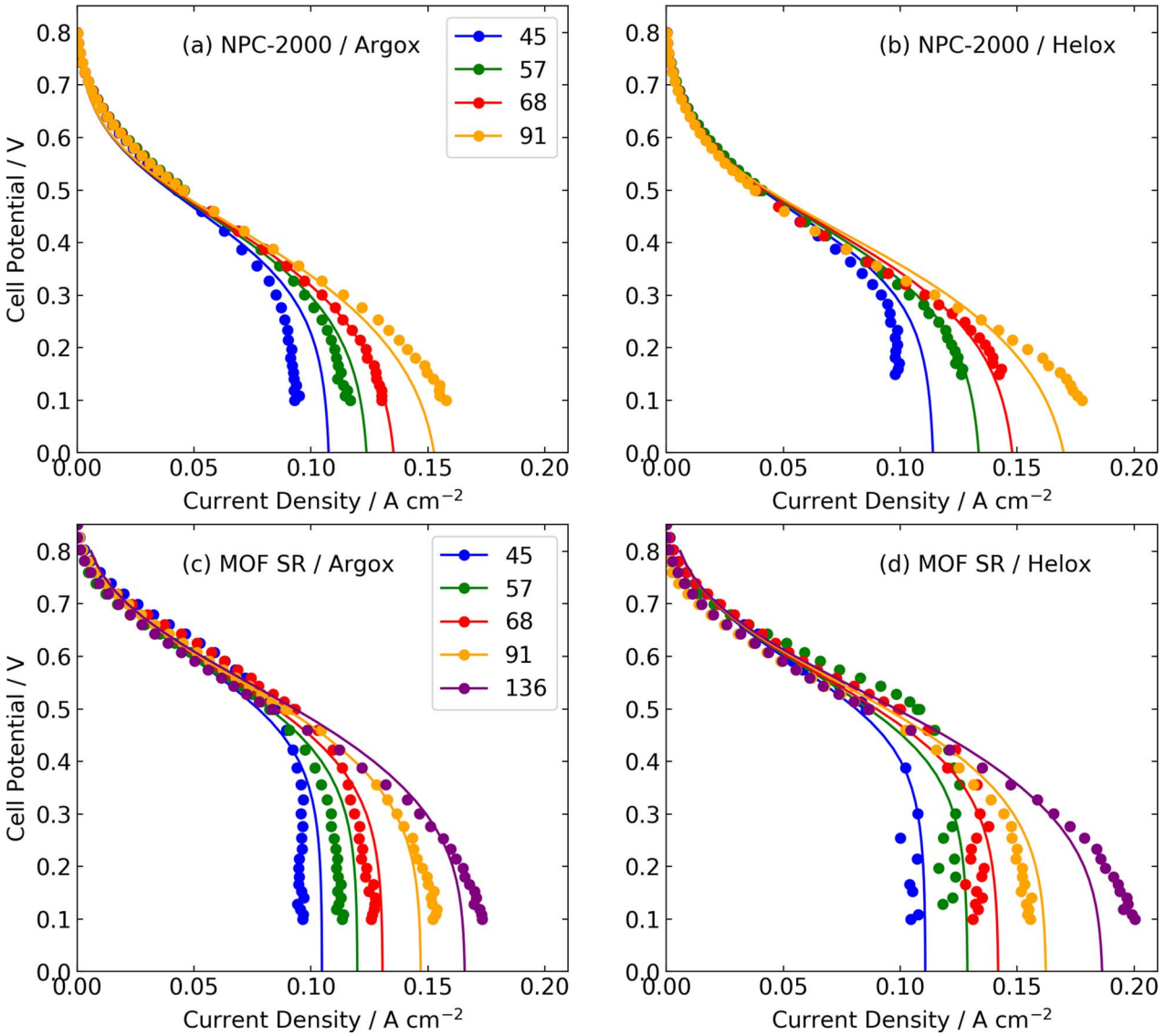

Figure 5. Comparison of experimental and model results at multiple flow rates for (a) NPC-2000 in argon (b) NPC-2000 in helium (c) MOF SR in argon (d) MOF SR in helium. Conditions: Temp. 80°C, 25BC GDL, 3mg/cm^2 Catalyst Loading, 45 wt% Nafion, Cell Area: 5cm^2, membrane: NR211.

mass transfer parameters, f_{HO} and k_{MT} are also similar within the confidence interval, reflecting nearly identical limiting current dependence on flow rate.

As shown in Fig. 5, the model results fit the experimental data reasonably well at high potentials, considering the spread in the data and accounting for two different carrier gases. At low potentials, it can be seen that the limiting currents predicted by the model do not vary as strongly with gas flow rate as do the experimental results. We attribute this difference to the isothermal nature of the model. In the experimental system, increased current density will raise the local temperature in the electrode, affecting various transport and reaction properties. This effect is not accounted for in the model.

Despite this deficiency, the values of k_{MT} obtained from the fits demonstrate a high correlation to the experimental data for both the MOF SR and the NPC-2000 catalyst, as shown in Fig. 6. The model captures the molecular weight dependence, as well as the intercept at $k_{MT}^{-1} \approx 300$ m^{-1} s.

Sensitivity Studies

Based on the model results shown in Fig. 6, sensitivity of the slope, k_g', and intercept, k_0, to a small set of parameters was analyzed. Parameters given in Table IV were considered, as well as three additional parameters: r_1 and r_2, representing the pore radii of MOF SR

Table IV. Model Fitting Parameters.

Fit Parameter	MOF SR	NPC-2000
Catalyst Layer Conductivity (κ, mS cm^{-1})	3.6 ± 0.55	3.3 ± 0.58
Catalyst Layer Exchange Current Density (i_0, A cm^{-3})	117 ± 25	91 ± 17
Catalyst Layer Hydrophobic Fraction (f_{HO})	0.30 ± 0.053	0.24 ± 0.043
Catalyst Layer Mass Transfer Coefficient (k_{MT}, mol cm^{-3} s^{-1})	0.11 ± 0.006	0.16 ± 0.28

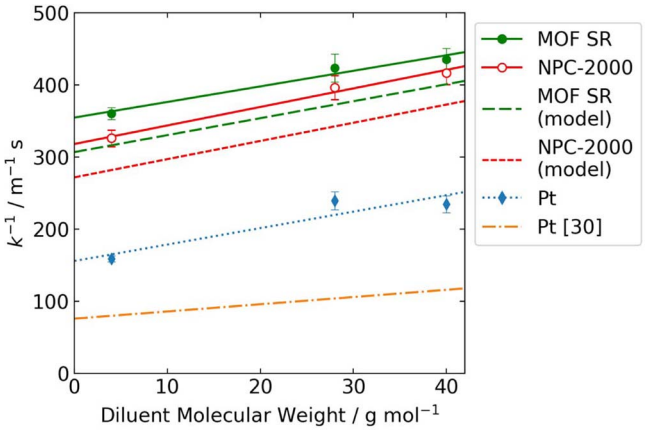

Figure 6. Comparison of experimental and model results demonstrating the linear correlation between the inverse of the mass transport coefficient and molecular weight of the diluent gas.

catalyst (173 and 277 nm, respectively, see Table I) and the catalyst layer thickness, L (79 μm).

Results of the sensitivity study, shown in Figure 7, indicate that both the slope and intercept are most sensitive to hydrophobic pore fraction, f_{HO}, the local mass transfer coefficient, k_{MT}, and the electrode thickness, L. The slope, k'_g, is most sensitive to f_{HO}, which controls the fraction of electrode available to gas phase transport. In contrast, the intercept, k_0, is most sensitive to the local mass transfer coefficient, k_{MT}, because that parameter represents the only restriction to mass transport as the diluent molecular weight, M, goes to zero. The parameters are equally and oppositely sensitive to the electrode thickness, L. The intercept, k_0, increases with L because of the increased effective area of the electrode. In contrast, the slope, k'_g, decreases with L because the thickness contributes to the path length over which transport occurs.

It is notable that negligible sensitivity to the pore radii, r_1 and r_2, was observed, indicating that Knudsen diffusion does not affect transport in this electrode. Similarly, the parameters are insensitive to changes in reaction kinetics or ohmic resistance, represented by the exchange current density i_0 and conductivity, κ, respectively. This suggests that both parameters are mass transfer controlled, most significantly the intercept, k_0.

These results reflect the value of using the pseudo-2D model to analyze these experimental results. In extrapolating model results to conditions unlimited by mass transfer, the impact of model parameters

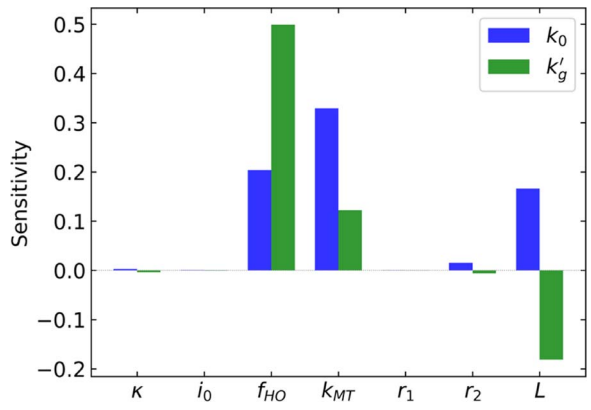

Figure 7. Model-calculated sensitivity of slope, k'_g, and intercept k_0 to key model parameters. Sensitivity is defined by Eq. 10 and parameter symbols are defined in text. The carrier gas-independent intercept k_0 is shown to be most sensitive to hydrophobic pore fraction, f_{HO}, the mass transfer coefficient k_{MT}, and the electrode thickness, L.

can be evaluated under those conditions. In this case, it is clear that performance at high rates may be improved by increasing hydrophobicity in the electrode and attention to mass transport barriers at the catalyst particle level.

Conclusions

Mass transport studies were carried out on a pair of non-PGM catalysts, revealing increased information regarding the mass transport resistances. Experiments were carried out by using a cathode gas comprised of oxygen diluted with an inert carrier gas. In this work, argon, nitrogen, and helium were used. Results indicated that both non-PGM catalysts showed comparable mass transport coefficients, and subsequently, mass transport resistances. However, the non-PGM materials both demonstrated significantly higher mass transport resistances than the Pt standard MEAs that were evaluated or referenced. This could largely be due to the significantly thicker catalyst layer present in non-PGM MEAs than is traditionally seen in Pt MEAs. Several trends were seen within the data, validating the results, given known trends in a Pt-based system. The argon and nitrogen-diluted gases showed virtually identical mass transport coefficients and resistances. The resistances of the argon and nitrogen-diluted gases were higher than that of helium, which would be expected as the oxygen should have an easier time in terms of transport through the carrier gas. Additionally, a previously developed model was adapted into a pseudo 2-D model to account for the oxygen depletion in the flow fields as a function of path length. This new model was combined with mercury intrusion porosimetry to predict the mass transport coefficients which were subsequently shown to be in agreement with the experimental data. Sensitivity studies extrapolating the model results to conditions unlimited by mass transfer allowed for additional info of individual model parameters and their general influence on the mass transfer parameters. This demonstrated the first use of these dilute oxygen experiments to elucidate information regarding the mass transport characteristics of non-PGM catalysts. Such work is crucial towards improving non-PGM-based fuel cell performance if they are to become commercially viable products.

Acknowledgments

The authors thank The Department of Energy, EERE (DE-EE-0000459).

ORCID

Ryan Pavlicek https://orcid.org/0000-0002-9229-5592

References

1. A. F. Gullá, M. S. Saha, R. J. Allen, and S. Mukerjee, "Toward Improving the Performance of PEM Fuel Cell by Using Mix Metal Electrodes Prepared by Dual IBAD." *J. Electrochem. Soc.*, **153**(2), A366 (2006).
2. N. Ramaswamy, T. M. Arruda, W. Wen, N. Hakim, M. Saha, A. Gullá, and S. Mukerjee, "Enhanced activity and interfacial durability study of ultra low Pt based electrocatalysts prepared by ion beam assisted deposition (IBAD) method." *Electrochim. Acta*, **54**(26), 6756 (2009).
3. S. Mukerjee, M. S. Saha, A. Gulla, and R. Allen, "Enhancing the Performance of Low Pt Loading Prepared by Dual Ion-Beam Assisted Deposition in PEM Fuel Cells." *ECS Trans.*, **1**(6), 77 (2006).
4. M. S. Saha, A. F. Gullá, R. J. Allen, and S. Mukerjee, "High performance polymer electrolyte fuel cells with ultra-low Pt loading electrodes prepared by dual ion-beam assisted deposition." *Electrochim. Acta*, **51**(22), 4680 (2006).
5. H. T. Chung, J. H. Won, and P. Zelenay, "Active and stable carbon nanotube/nanoparticle composite electrocatalyst for oxygen reduction." *Nat. Commun.*, **4**, 1922 (2013).
6. G. Wu, K. L. More, C. M. Johnston, and P. Zelenay, "High-Performance Electrocatalysts for Oxygen Reduction Derived from Polyaniline, Iron, and Cobalt." *Science*, **332**(6028), 443 (2011).
7. M. Lefèvre, E. Proietti, F. Jaouen, and J.-P. Dodelet, "Iron-Based Catalysts with Improved Oxygen Reduction Activity in Polymer Electrolyte Fuel Cells." *Science*, **324**(5923), 71 (2009).

8. E. Proietti, F. Jaouen, M. Lefèvre, N. Larouche, J. Tian, J. Herranz, and J.-P. Dodelet, "Iron-based cathode catalyst with enhanced power density in polymer electrolyte membrane fuel cells." *Nat Commun*, **2**, 416 (2011).
9. F. Charreteur, F. Jaouen, and J.-P. Dodelet, "Iron porphyrin-based cathode catalysts for PEM fuel cells: Influence of pyrolysis gas on activity and stability." *Electrochim. Acta*, **54**(26), 6622 (2009).
10. D. Deng, L. Yu, X. Chen, G. Wang, L. Jin, X. Pan, J. Deng, G. Sun, and X. Bao, "Iron Encapsulated within Pod-like Carbon Nanotubes for Oxygen Reduction Reaction." *Angew. Chem. Int. Ed.*, **52**(1), 371 (2013).
11. G. Faubert, G. Lalande, R. Côté, D. Guay, J. P. Dodelet, L. T. Weng, P. Bertrand, and G. Dénès, "Heat-treated iron and cobalt tetraphenylporphyrins adsorbed on carbon black: Physical characterization and catalytic properties of these materials for the reduction of oxygen in polymer electrolyte fuel cells." *Electrochim. Acta*, **41**(10), 1689 (1996).
12. M. Ferrandon, X. Wang, A. J. Kropf, D. J. Myers, G. Wu, C. M. Johnston, and P. Zelenay, "Stability of iron species in heat-treated polyaniline–iron–carbon polymer electrolyte fuel cell cathode catalysts." *Electrochim. Acta*, **110**, 282 (2013).
13. J. Herranz, F. Jaouen, and J.-P. Dodelet, "Electrochemical Evidence of Two Types of Active Sites for Oxygen Reduction in Fe-based Catalysts." *ECS Trans.*, **25**(1), 117 (2009).
14. F. Jaouen, F. Charreteur, and J. P. Dodelet, "Fe-Based Catalysts for Oxygen Reduction in PEMFCs." *J. Electrochem. Soc.*, **153**(4), A689 (2006).
15. F. Jaouen, E. Proietti, M. Lefevre, R. Chenitz, J.-P. Dodelet, G. Wu, H. T. Chung, C. M. Johnston, and P. Zelenay, "Recent advances in non-precious metal catalysis for oxygen-reduction reaction in polymer electrolyte fuel cells." *Energy Environ. Sci.*, **4**(1), 114 (2011).
16. U. I. Kramm, J. Herranz, N. Larouche, T. M. Arruda, M. Lefevre, F. Jaouen, P. Bogdanoff, S. Fiechter, I. Abs-Wurmbach, S. Mukerjee, and J.-P. Dodelet, "Structure of the catalytic sites in Fe/N/C-catalysts for O2-reduction in PEM fuel cells." *PCCP*, **14**(33), 11673 (2012).
17. Q. Li, H. Pan, D. Higgins, R. Cao, G. Zhang, H. Lv, K. Wu, J. Cho, and G. Wu, "Metal–Organic Framework-Derived Bamboo-like Nitrogen-Doped Graphene Tubes as an Active Matrix for Hybrid Oxygen-Reduction Electrocatalysts." *Small*, **11**(12), 1443 (2015).
18. L. Qu, Y. Liu, J.-B. Baek, and L. Dai, "Nitrogen-Doped Graphene as Efficient Metal-Free Electrocatalyst for Oxygen Reduction in Fuel Cells." *ACS Nano*, **4**(3), 1321 (2010).
19. J. Tian, L. Birry, F. Jaouen, and J. P. Dodelet, "Fe-based catalysts for oxygen reduction in proton exchange membrane fuel cells with cyanamide as nitrogen precursor and/or pore-filler." *Electrochim. Acta*, **56**(9), 3276 (2011).
20. U. Tylus, Q. Jia, K. Strickland, N. Ramaswamy, A. Serov, P. Atanassov, and S. Mukerjee, "Elucidating Oxygen Reduction Active Sites in Pyrolyzed Metal–Nitrogen Coordinated Non-Precious-Metal Electrocatalyst Systems." *J. Phys. Chem. C*, **118**(17), 8999 (2014).
21. A. Serov, K. Artyushkova, E. Niangar, C. Wang, N. Dale, F. Jaouen, M.-T. Sougrati, Q. Jia, S. Mukerjee, and P. Atanassov, "Nano-structured non-platinum catalysts for automotive fuel cell application." *Nano Energy*, **16**, 293 (2015).
22. A. Serov, K. Artyushkova, and P. Atanassov, "Fe-N-C Oxygen Reduction Fuel Cell Catalyst Derived from Carbendazim: Synthesis, Structure, and Reactivity." *Adv. Energy Mater.*, **4**(10), (2014).
23. A. Serov, M. J. Workman, K. Artyushkova, P. Atanassov, G. McCool, S. McKinney, H. Romero, B. Halevi, and T. Stephenson, "Highly stable precious metal-free cathode catalyst for fuel cell application." *J. Power Sources*, **327**, 557 (2016).
24. K. Strickland, E. Miner, Q. Jia, U. Tylus, N. Ramaswamy, W. Liang, M.-T. Sougrati, F. Jaouen, and S. Mukerjee, "Highly active oxygen reduction non-platinum group metal electrocatalyst without direct metal-nitrogen coordination." *Nat. Commun.*, **6**, (2015).
25. N. Ramaswamy and S. Mukerjee, "Fundamental Mechanistic Understanding of Electrocatalysis of Oxygen Reduction on Pt and Non-Pt Surfaces: Acid versus Alkaline Media." *Adv. Phys. Chem.*, **2012**, 17 (2012).
26. D. R. Baker, D. A. Caulk, K. C. Neyerlin, and M. W. Murphy, "Measurement of Oxygen Transport Resistance in PEM Fuel Cells by Limiting Current Methods." *J. Electrochem. Soc.*, **156**(9), B991 (2009).
27. D. A. Caulk and D. R. Baker, "Heat and Water Transport in Hydrophobic Diffusion Media of PEM Fuel Cells." *J. Electrochem. Soc.*, **157**(8), B1237 (2010).
28. R. Makharia, M. F. Mathias, and D. R. Baker, "Measurement of Catalyst Layer Electrolyte Resistance in PEFCs Using Electrochemical Impedance Spectroscopy." *J. Electrochem. Soc.*, **152**(5), A970 (2005).
29. H. Liu, W. K. Epting, and S. Litster, "Gas Transport Resistance in Polymer Electrolyte Thin Films on Oxygen Reduction Reaction Catalysts." *Langmuir*, **31**(36), 9853 (2015).
30. T. V. Reshetenko and J. St-Pierre, "Separation Method for Oxygen Mass Transport Coefficient in Gas and Ionomer Phases in PEMFC GDE." *J. Electrochem. Soc.*, **161**(10), F1089 (2014).
31. Y. W. Rho, S. Srinivasan, and Y. T. Kho, "Mass Transport Phenomena in Proton Exchange Membrane Fuel Cells Using O_2/He, O_2/Ar, and O_2/N_2 Mixtures: II. Theoretical Analysis." *J. Electrochem. Soc.*, **141**(8), 2089 (1994).
32. Y. W. Rho, O. A. Velev, S. Srinivasan, and Y. T. Kho, "Mass Transport Phenomena in Proton Exchange Membrane Fuel Cells Using O_2/He, O_2/Ar, and O_2/N_2 Mixtures: I. Experimental Analysis." *J. Electrochem. Soc.*, **141**(8), 2084 (1994).
33. N. D. Leonard, K. Artyushkova, B. Halevi, A. Serov, P. Atanassov, and S. C. Barton, "Modeling of Low-Temperature Fuel Cell Electrodes Using Non-Precious Metal Catalysts." *J. Electrochem. Soc.*, **162**(10), F1253 (2015).
34. A. W. Adamson and A. P. Gast, *Physical chemistry of surfaces*, 6th ed.; New York: Wiley: New York, 1997.
35. C. C. M. Luijten, K. J. Bosschaart, and M. E. H. Van Dongen, "A new method for determining binary diffusion coefficients in dilute condensable vapors." *Int. J. Heat Mass Transfer*, **40**(15), 3497 (1997).
36. T. R. Marrero and E. A. Mason, "Gaseous Diffusion Coefficients." *J. Phys. Chem. Ref. Data*, **1**(1), 3 (1972).
37. B. E. Poling, *The properties of gases and liquids*, 5th ed. ed.; New York: McGraw-Hill: New York, 2001.
38. H. S. Fogler, *Elements of chemical reaction engineering*, Fifth edition. ed.; Boston: Prentice Hall: 2016.
39. Q. Jia, N. Ramaswamy, U. Tylus, K. Strickland, J. Li, A. Serov, K. Artyushkova, P. Atanassov, J. Anibal, C. Gumeci, S. C. Barton, M.-T. Sougrati, F. Jaouen, B. Halevi, and S. Mukerjee, "Spectroscopic insights into the nature of active sites in iron–nitrogen–carbon electrocatalysts for oxygen reduction in acid." *Nano Energy*, **29**, 65 (2016).
40. S. L. Seager, L. R. Geertson, and J. C. Giddings, "Temperature Dependence of Gas and Vapor Diffusion Coefficients." *J. Chem. Eng. Data*, **8**(2), 168 (1963).